

Algorithm Theoretical Basis Document for the GOME-2 Rapid Volcanic SO₂ product

Andreas Richter
Institute of Environmental Physics
University of Bremen
Germany

Document Version: First Draft

Last changed: October 5th, 2009



Table of contents

1	Introduction.....	4
1.1	Scope of document.....	4
1.2	The SAVAA project.....	4
1.3	UV/vis SO ₂ measurements from satellite	4
1.4	The GOME-2 instrument.....	5
2	SO ₂ Measurement Sensitivity	5
2.1	Dependence on altitude	6
2.2	Dependence on wavelength and solar zenith angle	7
2.3	Dependence on ozone column	7
2.4	Dependence on SO ₂ total column amount	8
2.5	Dependence on surface reflectivity.....	9
2.6	Averaging kernels	9
2.7	Requirements for SO ₂ retrieval	10
3	SO ₂ Algorithm	10
3.1	DOAS fit.....	10
3.2	Iterative Column Selection.....	12
3.3	Iterative spike correction.....	13
3.4	Post Processing.....	15
3.5	Error Discussion and Validation	16
4	Retrieval Example: Kasatochi eruption August 2008.....	16
5	Planned Improvements	17
6	Volcanic Alert System.....	17
6.1	Identification of volcanic plumes	17
6.2	Web interface.....	18
6.3	Open issues / plans for improvements.....	19
7	Data Formats	19
7.1	Format of swath files	20

7.2	Format of alert files	21
8	Acronyms.....	21
9	References.....	21

1 Introduction

1.1 Scope of document

In this document, a brief introduction is given to the basics of satellite measurements of SO₂ using Differential Optical Absorption Spectroscopy (DOAS) in the UV part of the spectrum. The sensitivity of the measurements as function of SO₂ amount, SO₂ vertical profile, surface albedo and other parameters is discussed and the retrieval algorithm developed at the University of Bremen for the near real time (NRT) retrieval of volcanic SO₂ from GOME-2 measurements is described. The description is complemented by a short introduction of the web based volcanic alert system using the new data product and a definition of the file formats of the output data.

1.2 The SAVAA project

The SAVAA (Support to Aviation for Volcanic Ash Avoidance) project is an ESA funded project aiming at the development of a demonstration system using various satellite data in combination with forward and inverse trajectory modelling to provide VAACs with information on volcanic plumes. Both ash and SO₂ products are included as well as a combination of IR and UV sensors. As VAACs need volcanic information in NRT, geostationary observations are the most appropriate data source. So far, no UV instruments with sufficient spectral resolution are available on such platforms. Therefore, UV retrievals of SO₂ are mainly used for validation of IR retrievals and to constrain plume evolution for inverse modelling of plume altitude. However, even for these applications a fast delivery of the products is needed, limiting the complexity of retrieval schemes.

More information on the SAVAA project can be found at <http://savaa.nilu.no/>.

1.3 UV/vis SO₂ measurements from satellite

The SO₂ molecule has strong absorption bands in the UV part of the solar spectrum (see. Fig. 1). These features can be used to remotely sense atmospheric SO₂ amounts by applying absorption spectroscopy to measurements of scattered sunlight.

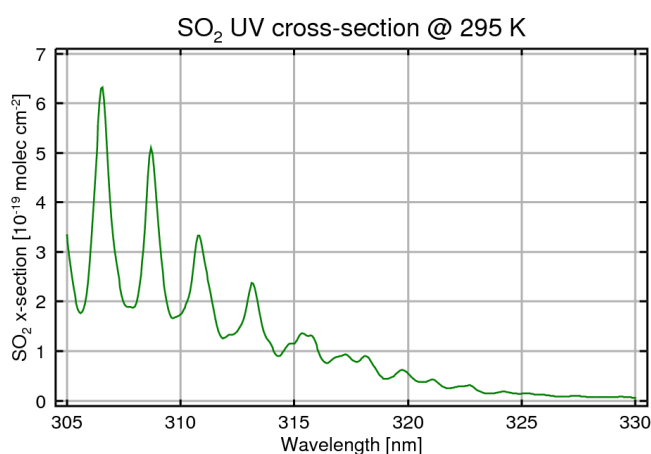


Fig. 1: SO₂ absorption cross-section (Vandaele et al., 1994) convoluted with the GOME-2 slit function

First satellite observations of volcanic SO₂ were reported by Krueger (1983) using data from the TOMS instrument which has only a few spectral bands limiting sensitivity to strong eruptions.

However, the long time series available in combination with the relatively good spatial resolution of the instrument provides a useful long-term record of satellite observed SO₂ from space (Krueger et al., 1995, Carn et al., 2003). Volcanic SO₂ could also be detected using the SBUV/2 instrument (McPeters, 1993). The improved spectral resolution of the GOME instrument launched in 1995 on ERS-2 reduced the detection limit for SO₂ retrievals facilitating detection of weaker signals including tropospheric pollution (Eisinger and Burrows, 1998, Khokhar et al., 2004, Thomas et al., 2005). In 2002, the SCIAMACHY instrument followed providing smaller ground-pixels but reduced spatial coverage (Afe et al., 2004, Richter et al., 2006, Lee et al., 2008, Lee et al., 2009). The OMI instrument, launched in 2004, combines high spatial resolution with daily global coverage and high spectral resolution. Sulphur dioxide signals from volcanic eruptions and pollution have been retrieved from OMI measurements using different algorithms, (e.g. Krotkov, 2006, Carn et al., 2007, Yang et al., 2009a, Krotkov et al., 2009) including high volcanic SO₂ loadings (Yang et al., 2007) and the retrieval of volcanic plume height (Yang et al. 2009b).

For the rapid volcanic SO₂ product described here, data from the GOME-2 instrument are used.

1.4 The GOME-2 instrument

The GOME-2 instrument is a 4 channels UV / visible spectrometer covering the spectral region from 240 to 790 nm with a spectral resolution of 0.26 to 0.51 nm (Munro et al., 2006). It was launched on MetOp-A in October 2006 and has been providing measurements since January 2007. The MetOp-A satellite is in a near polar sun-synchronous orbit with a descending node equator crossing time of 09:30 LT. The GOME-2 instrument is observing the upwelling radiance from the atmosphere in near nadir observation geometry. It has a large swath of 1920 km, resulting in global coverage at the equator in 1.5 days and several overpasses per day at higher latitudes. The spatial resolution of the forward scan measurements is 80 x 40 km² over most of the globe but is reduced at large solar zenith angle to improve signal to noise ratio. During the rapid back scan, spatial resolution is reduced to 320 x 40 km² and these data is not used here. In regular intervals, GOME-2 is operating in “narrow swath mode” which improves spatial resolution by a factor of 6 but reduces coverage. Once per day, the instrument takes a direct sun measurement which is used as absorption free background spectrum.

The GOME-2 instrument is based on the GOME instrument launched on ERS-2 in April 1995. It has a very similar optical layout but some important improvements, including better spatial resolution, better coverage and reduced sensitivity to the polarisation of the incoming light. The current GOME-2 instrument is the first in a series of three identical instruments to be launched in sequence and providing a consistent long-term data set of operational UV / visible observations. More information on the GOME-2 instrument can be found at the following internet pages:

- IUP Bremen GOME-2 page (<http://www.doas-bremen.de/GOME-2.htm>)
- ESA GOME-2 page (http://www.esa.int/esaLP/SEMTEG23IE_LPmetop_0.html)
- DLR GOME-2 page (<http://wdc.dlr.de/sensors/gome2/>)

2 SO₂ Measurement Sensitivity

The sensitivity of satellite nadir measurements in the UV depends on many parameters, of which the most important ones will briefly be discussed here. The signal received at the satellite sensor is comprised of photons scattered by air molecules, photons scattered by aerosols or clouds and light

reflected on the surface. Only the last group of photons will have passed through the complete atmosphere whereas the scattered photons do not probe the atmosphere below the scattering point (see Fig. 2). As a result, the measurements are less sensitive to absorption in the lower atmosphere. Any effect that changes the relative contributions of photons from different altitudes will affect the measurement sensitivity. For example, a brighter surface will increase the proportion of reflected photons increasing sensitivity. A cloud will reduce sensitivity below it but will increase sensitivity above its top. Strong extinction by Rayleigh scattering, aerosols or absorbers such as ozone will reduce the sensitivity to lower layers thereby affecting the wavelength dependence of the sensitivity. Overall a complex behaviour follows which will have to be accounted for in the retrieval to get accurate results.

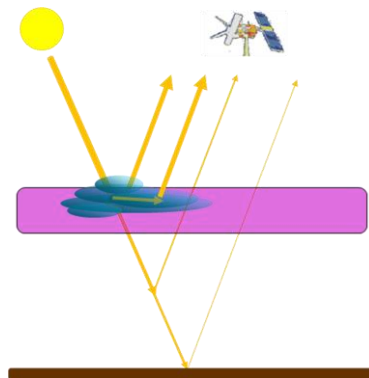


Fig. 2: Sketch of the observing geometry and the different contributions to the observed signal assuming single scattering only

2.1 Dependence on altitude

As mentioned above, strong Rayleigh scattering in combination with ozone absorption reduces the sensitivity towards the surface in particular for low surface albedo. This is illustrated in Fig. 3 for two wavelengths and three total SO₂ column amounts. While above 10 km, the sensitivity is relatively constant, it strongly reduces to the surface where it is very small. At large SO₂ columns, the effect is enhanced at the shorter wavelengths (see discussion below).

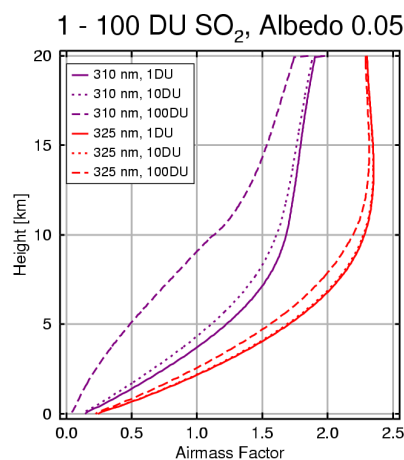


Fig. 3: Vertical sensitivity for two wavelengths and three SO₂ loadings at 40° SZA and a surface albedo of 0.05. The SO₂ was assumed to be evenly distributed from the surface to 10 km.

2.2 Dependence on wavelength and solar zenith angle

The sensitivity of the measurements also depends on solar zenith angle. Several effects contribute to this dependency: First, the absorption increases as the light path through the SO₂ layer increases at low sun for purely geometric reasons. Second, the extinction by Rayleigh scattering and ozone and SO₂ absorption increases with increasing SZA reducing the sensitivity in particular to the shorter wavelengths. Third, the radiance received at the satellite sensor decreases with increasing SZA as result of the larger extinction which increases the measurement noise. The last point ultimately limits the useful range of SZAs for SO₂ retrieval and thereby the coverage of the satellite measurements.

The effects of SZA on the light path are illustrated in Fig. 4 as a function of wavelength for a moderate SO₂ column of 10 DU. As can be seen, the airmass factors increase with SZA but towards shorter wavelengths, the extinction becomes increasingly important leading to an actual reversal of the order at 314 nm.

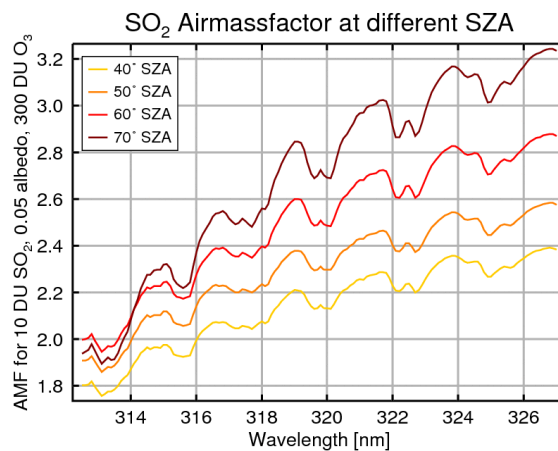


Fig. 4: Wavelength and SZA dependence of the SO₂ airmass factor for a 10 DU SO₂ layer of 1 km thickness between 10 and 11 km. Surface albedo was set to 0.05 and a 300 DU US standard ozone profile was assumed.

2.3 Dependence on ozone column

For standard DOAS applications, the spectral fitting and the correction for light path are separated. This is possible in the case of weak absorption where one can assume that the atmospheric radiation field is not affected significantly by the amount and vertical distribution of the trace gas. For these situations, the DOAS retrieval provides the slant column of the absorber which is then converted by a single number, the airmass factor (AMF) to the vertical column. However, in the UV ozone absorption is large and the average light path varies with wavelength as a function of the ozone absorption cross-section. Also, Rayleigh scattering strongly affects the signal leading to a rapid change of light path with wavelength.

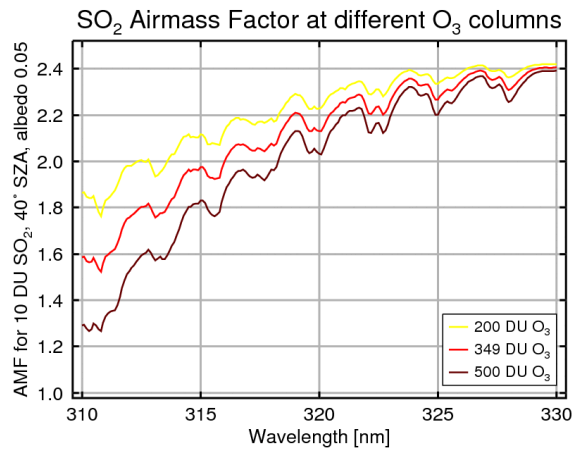


Fig. 5: Wavelength dependence of the SO_2 airmass factor for different ozone columns. A 10 DU SO_2 layer of 1 km thickness between 10 and 11 km was used, surface albedo was set to 0.05 and SZA was 40° .

In Fig. 5, the effect is illustrated for three different ozone columns. As can be seen, the light path decreases towards shorter wavelengths as result of increased Rayleigh scattering and ozone absorption. Also, the spectral signature of the ozone absorption cross-section is reflected in the SO_2 airmass factor as variations in ozone absorption with wavelength lead to variations in average light path length. Both effects increase for increasing ozone column. Overall the effect is negligible at longer wavelengths but can be as large as 20% at 310 nm.

2.4 Dependence on SO_2 total column amount

At large SO_2 columns, the absorption of SO_2 itself becomes significant and changes the average light path. As shown in Fig. 6, the AMF decreases with increasing SO_2 column, in particular at short wavelengths. At the same time, the spectral signature of the SO_2 absorption cross-section becomes apparent in the AMF on top of the ozone structures which leads to a distortion of the absorption signature of SO_2 if not accounted for.

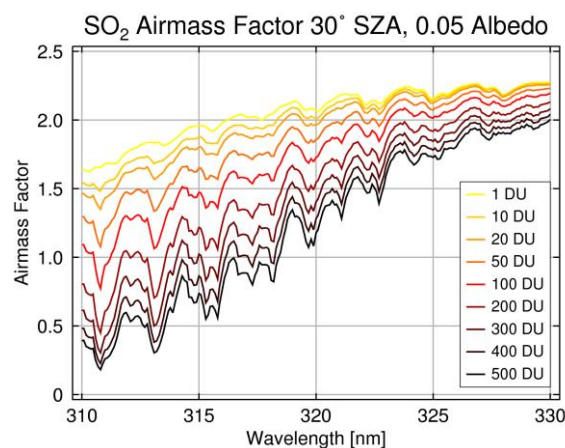


Fig. 6: Dependence of SO_2 airmass factor on SO_2 column in a 1 km thick layer between 10 and 11 km. Surface albedo was set to 0.05, ozone column to 300 DU and SZA is 30° .

2.5 Dependence on surface reflectivity

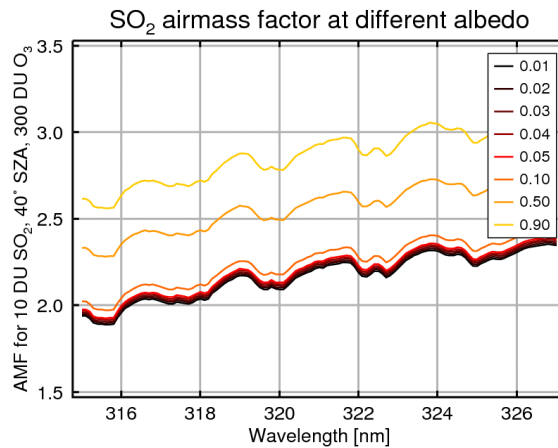


Fig. 7: Dependence of SO₂ airmass factor on surface albedo for a 1 km thick layer of 10 DU SO₂ between 10 and 11 km. The ozone column to 300 DU and SZA is 40°.

Surface reflectivity also plays a significant role in the sensitivity of the measurements towards SO₂. This includes two aspects – first the increased intensity over bright surfaces which reduces the noise of the measurements and second the increase in light path over reflective surfaces. The latter effect is illustrated in Fig. 7 where the airmass factor for a 1 km thick SO₂ layer between 10 and 11 km is shown for different surface albedos. As can be seen, only very large albedos have an impact for this scenario, making albedo effects important only over snow and ice as well as over bright surfaces. In contrast, for low layers of SO₂ as are found in the situation of anthropogenic pollution, dependence on surface albedo is very large (not shown).

2.6 Averaging kernels

For many satellite data products, averaging kernels are provided to the users to facilitate interpretation and quantitative comparison to other data sets. The idea of the averaging kernel is to provide the information, on how much the retrieved value for altitude layer i is changed if the true atmospheric profile in layer j is changed by a certain amount. In the case of column products, this simplifies to the question of how much the retrieved vertical column changes if the true profile changes by a given amount in layer j .

The averaging kernels are computed from the weighting functions, in the case of column products by simply dividing the altitude dependent airmass factors by the overall airmass factor (Eskes and Boersma, 2003). However, the weighting function is valid only in cases where the radiative transfer is sufficiently linear for changes in the absorber concentration. For large SO₂ amounts, this is not the case.

As an example, consider a layer of 100 DU SO₂ at 12 km. As the absorption is quite strong, the sensitivity below this layer at e.g. 10 km will be very small, and this will be reflected in small weighting functions and averaging kernels computed for a scenario assuming such an SO₂ profile. However, if the real SO₂ layer is at 10 km instead of 12 km, no such shielding exists and the real sensitivity at 10 km is nearly as high as it was at 12 km in the first scenario.

As a result, the weighting function and the averaging kernels are ill defined and cannot be provided with the product. If the SO₂ column for an *a priori* vertical SO₂ profile differing from the one used in the retrieval is to be determined, a full radiative transfer calculation has to be performed.

2.7 Requirements for SO₂ retrieval

Based on the sensitivity studies shown above, the accuracy of a volcanic SO₂ retrieval depends critically on appropriate *a priori* assumptions for SO₂ amount and SO₂ layer altitude. Ozone column and surface reflectivity are also important, as well as proper treatment of clouds. As the air mass factor depends strongly on wavelength and in addition has spectral structures correlated to the SO₂ absorption cross-section, a standard DOAS retrieval will not be appropriate.

As discussed in Yang et al., 2009b, a full retrieval of the spectral information can provide information on all of the above parameters, leading to accurate and self-contained retrievals. However, such an inversion is slow and currently not applicable for a NRT product. In the next section, the retrieval approach used here is described.

3 SO₂ Algorithm

The SO₂ retrieval algorithm used for the SAVAA project was developed to be fast and adapted to volcanic eruptions. It is not optimised for the retrieval of SO₂ from pollution or volcanic degassing, and in its current form it is fast but not as accurate as possible.

The overall retrieval is performed in several steps which are the DOAS fit, an iterative SO₂ column selection, an iterative spike correction and a post processing performed on a complete orbit of data. The individual steps of the analysis are described in detail below.

3.1 DOAS fit

The DOAS (Differential Optical Absorption Spectroscopy) method is based on application of Beer Lambert's law of extinction to atmospheric measurements. The basic assumption in DOAS retrievals is the separation of spectral fitting of the absorption signal and determination of light path length. The signal observed by the detector $I(\lambda)$ is modelled as being proportional to the initial intensity ($I_0(\lambda)$) attenuated by absorption and scattering in the atmosphere:

$$I(\lambda) = I_0(\lambda)\alpha \exp \left\{ - \int \sigma(\lambda)\rho(s)ds - \sigma_{Ray}(\lambda) \int \rho_{Ray}(s)ds - \sigma_{Mie}(\lambda) \int \rho_{Mie}(s)ds \right\}$$

where σ_{Ray} is the Rayleigh extinction cross-section, σ_{Mie} is the Mie extinction cross-section and ρ_{Ray} and ρ_{Mie} are the number densities of Rayleigh and Mie scatterers, respectively. For simplicity, only one absorber is shown having the absorption cross-section σ . Integration is performed over the atmospheric light path s and α is a factor accounting for the scattering efficiency. In standard DOAS, the assumption is made that the light path does not depend on wavelength λ at least over a sufficiently small wavelength interval and the slant column density

$$SCD = \int \rho(s)ds$$

is defined which is the total amount of absorber per unit area integrated along the light path. Using this quantity and approximating the effects of scattering and broad band absorption by a polynomial, the DOAS equation can be derived

$$\ln \frac{I_0(\lambda)}{I(\lambda)} = \sum_i \sigma'_i(\lambda)SCD_i + \sum_p c_p \lambda^p$$

which links the measured intensities to the known absorption cross-sections in a system of linear equations which can be solved for the SCDs using least square methods.

The vertical column density VCD, which is defined as the vertical integral over absorber density

$$VCD = \int_0^{TOA} \rho(z) dz$$

is then derived by applying an airmass factor AMF which is defined by the ratio

$$AMF = \frac{SCD}{VCD}$$

and is computed with radiative transfer programs.

For large SO₂ columns, the assumption of a wavelength independent light path does not hold. Therefore, the DOAS equation has to be modified by replacing the SCDs with slant optical densities (SODs) which are defined as the integral over the product of absorption cross-section and absorber concentration:

$$SOD(\lambda) = \int \sigma(\lambda) \rho(s) ds$$

Using the SOD, the DOAS equation becomes

$$\ln \frac{I_0(\lambda)}{I(\lambda)} = \sum_i SOD_i(\lambda) + \sum_p c_p \lambda^p$$

where the SODs have to be computed using radiative transfer code. This equation will only be correct if the real atmosphere is identical to the one used in the calculations. For application in retrievals, the assumption is made that the SOD can be approximated by simple scaling of the modelled SOD⁰:

$$\ln \frac{I_0(\lambda)}{I(\lambda)} = \sum_i r_i SOD_i^0(\lambda) / VCD_i^0 + \sum_p c_p \lambda^p$$

This will work for small differences between real and assumed atmosphere. In case of large differences, a more appropriate *a priori* will have to be used and the procedure be repeated. How this iterative scheme is implemented here is described in the next section. By dividing the SOD_i by the model vertical column VCD_i⁰, the scaling factor r_i is identical to the vertical column to be retrieved.

The detailed settings selected for GOME-2 SO₂ fits are summarised in Tab. 1.

Parameter	Setting
Fitting window	312.5 – 327 nm
Ozone	SOD for US standard atmosphere using GOME-2 FM absorption cross-sections + orthogonal temperature dependence from GOME-2 measurements at 243 and 273K
SO ₂	See Tab. 2
Ring effect	Vountas et al, 1998
Polynomial	Cubic (4 coefficients)
Additional corrections	Offset and slope
Background spectrum	GOME-2 daily solar measurement

Tab. 1: DOAS settings used for the GOME-2 SO₂ retrieval

3.2 Iterative Column Selection

As discussed above, the spectral shape of the SO₂ absorption as well as the absorption depth depend in a non-linear way on the total SO₂ amount present in the atmosphere. To account for this in a fast and simple manner, SODs have been tabulated for a number of wavelengths, solar zenith angles and SO₂ columns using a standard atmospheric scenario where only the total SO₂ amount varies. The scenarios used are summarised in Tab. 2.

Parameter	Value
SZA	1, 10, 20, 30, 40, 45, 50, 55, 60, 65, 70, 7 ₂ .5, 75, 76, 77, 78, 79, 80, 81, 8 ₂ , 83, 84, 85, 86, 87, 88, 89, 90, 91
LOS viewing angle	0 (nadir)
SO ₂ profile	Block profile between 10 and 11 km
SO ₂ total amount	1, 5, 10, 20, ...500 DU
Ozone profile	US standard
Surface albedo	0.05
Aerosols	none
Clouds	none

Tab. 2: Radiative transfer settings used for the tabulated SO₂ SODs

In the retrieval, the first iteration is performed using the SOD from the base scenario having an SO₂ column of 1 DU. If the retrieved column is larger than 4 DU, a second iteration is performed using the a priori column closest to the retrieved column. This procedure is repeated until the fit quality does not improve anymore. In this case, a last iteration step is taken using the mid-value between the last and the second to last SO₂ column. Based on the chisquare of this value, either the result of the second to last or the intermediate column is used as final result. A flow chart of the retrieval is shown in Fig. 8.

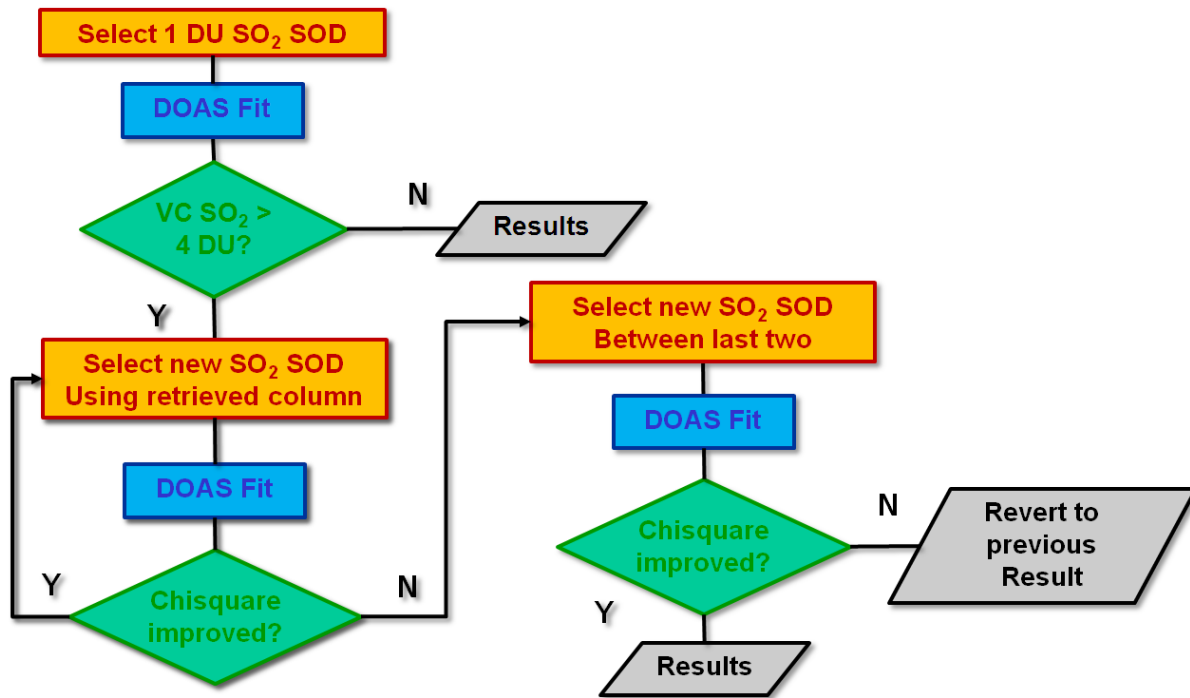


Fig. 8: Schematic of the iteration of the SO_2 column used for the a priori in the DOAS retrieval

Using this procedure, consistency in the columns of retrieval and a priori is assured, and a large fraction of the non-linearity in SO_2 absorption occurring is corrected. The procedure always converges as the behaviour of the SO_2 absorption as a function of SO_2 column is monotonous and the procedure is stopped when 500 DU are reached.

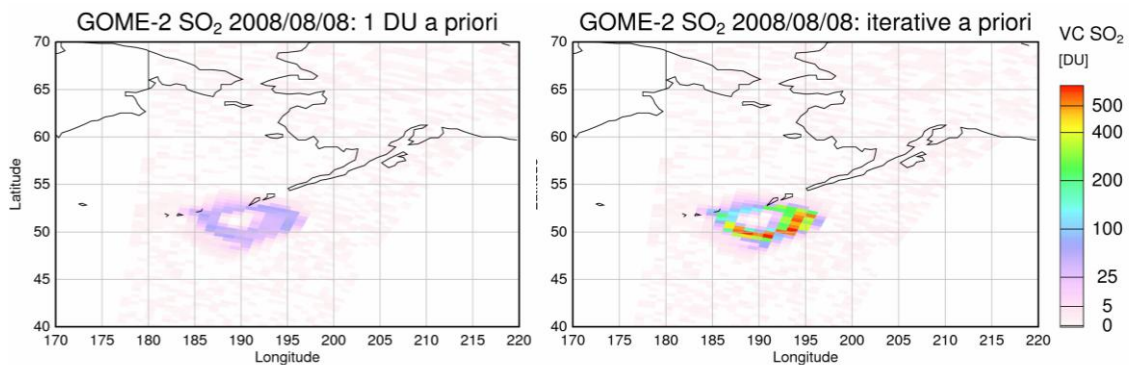


Fig. 9: Effect of iterative selection of SO_2 a priori used for the Kasatochi eruption plume on August 8, 2008 in GOME-2 data. Much larger SO_2 columns are retrieved with the iterative a priori in the centre of the plume. Note the logarithmic colour scale.

3.3 Iterative spike correction

An additional complication of the SO_2 retrieval arises from the fact that some GOME-2 spectra are affected by increased noise in some detector pixels. In the region of the South Atlantic Anomaly (SAA) where an anomaly in the Earth's magnetic field strongly increases the flux of fast particles, many spectra are affected resulting in increased noise and large scatter of the SO_2 columns. In other regions of the globe, much less spectra are affected.

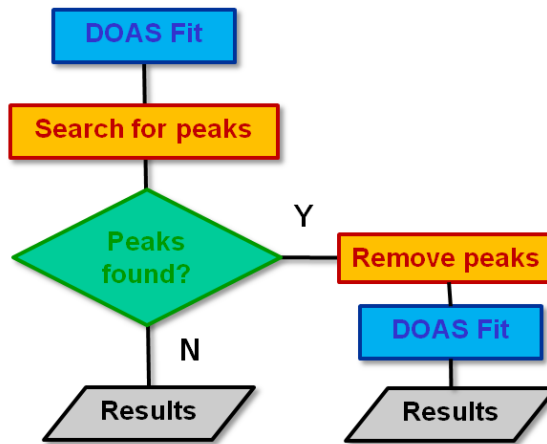


Fig. 10: Schematic of spike correction algorithm

While the increased noise is too small to be directly identified in the raw spectra, it can readily be seen in the fitting residuals as shown in Fig. 11. If the number of pixels which are affected is not too large, they can be identified in the residuals, flagged as having large errors and then the retrieval can be repeated. This approach has been taken here and results in a significant reduction of scatter in the SO₂ columns close to the SAA. The remaining scatter results from noise in the spectra which is below the threshold for spike removal but still interferes with the SO₂ retrieval.

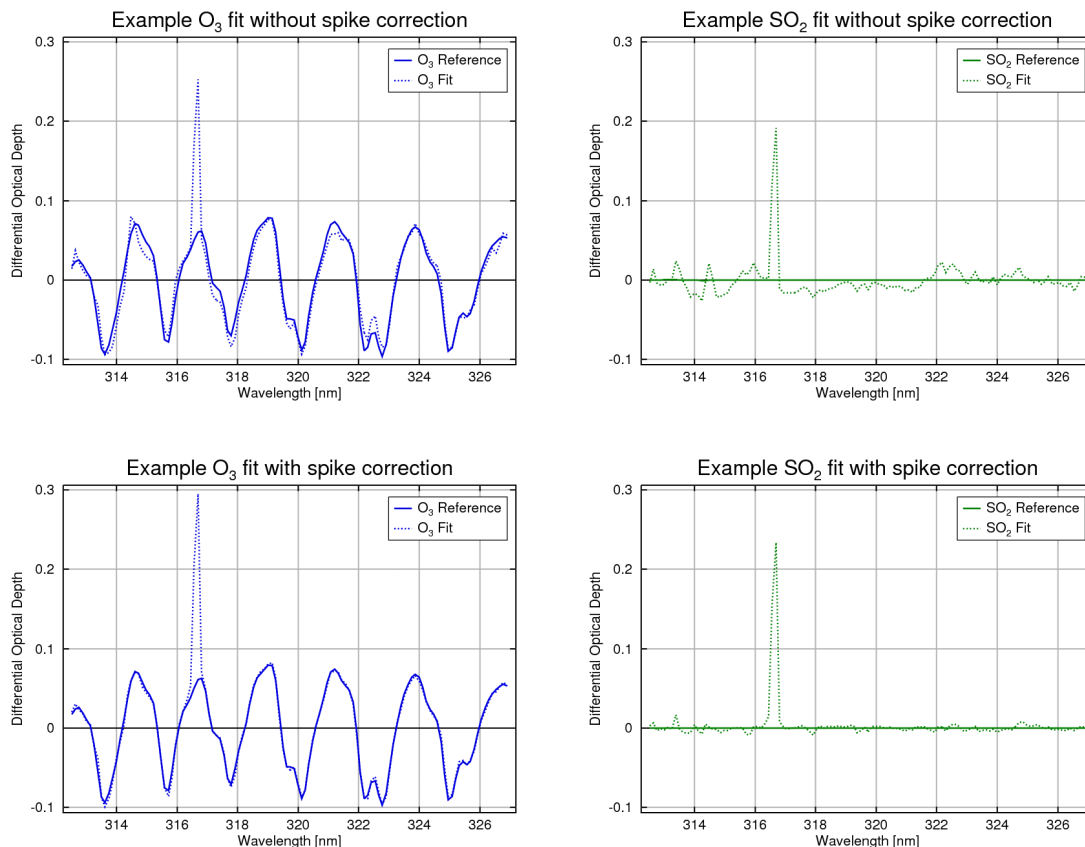


Fig. 11: Example of a fit result in the SAA affected by a spike without (upper panel) and with (lower panel) correction. The spike is not removed but a large uncertainty has been assigned to the affected values resulting in a much better ozone fit as well as a smaller residual in the SO₂ retrieval (no significant SO₂ was retrieved).

3.4 Post Processing

A well known problem in SO₂ retrievals from UV measurements is the presence of offsets in the data which results in non-zero columns even over region which are known to have very low SO₂. The origins of these offsets are not well understood but they vary with season and latitude, depend on the exact spectral region used and also on ozone columns. Possible explanations are residual instrumental straylight, interference by the strong ozone absorption or its temperature dependence or not fully compensated effects of rotational Raman scattering on air molecules.

Several different approaches have been proposed to correct for these offsets, including subtraction of a reference region over the Pacific (Richter et al., 1996), empirical corrections scaled to the ozone field (DLR 2009) and high pass filtering along individual orbits (Krotkov et al., 2006). Here, we have implemented a correction scheme using the last option.

The procedure used first attempts to remove the “real” high SO₂ values from the measurements of one orbit, and then computes the median of the remaining signal over a certain latitude range. These smoothed background values are then removed from all measurements of the orbit to force it to be close to zero with the exception of real volcanic signals. To compensate possible across track differences, the procedure is performed independently for each scan position of GOME-2. In the current implementation, the median is taken over 51 scan positions along track which corresponds to roughly 20 degrees latitude. An example of the background removal procedure is given in Fig. 12.

The background correction is less reliable at low sun where the scatter in GOME-2 SO₂ columns becomes very large and the number of measurements decreases as GOME-2 integration time is increasing stepwise. Possibilities for improved correction using more than one orbit are currently being investigated.

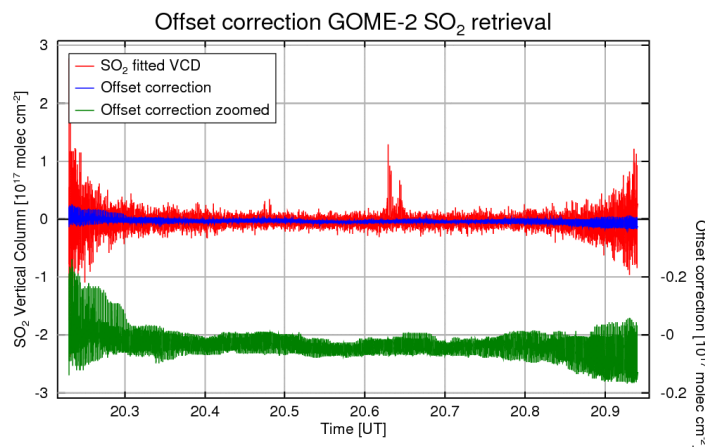


Fig. 12: Example of the background removal procedure applied to each orbit of GOME-2 SO₂ retrievals. The red curve is the original data, the blue curve the offset correction. The green curve is a zoomed version of the blue curve showing that the magnitude of the correction is small in comparison to the volcanic signals.

A conceptual problem with the background correction is the underlying assumption that SO₂ from volcanoes can be identified as relatively sharp enhancements. In case of large eruptions which inject SO₂ into the stratosphere, transport and mixing will lead to an enhanced stratospheric background level in SO₂ which cannot easily be separated from the type of retrieval offset corrected for by the background subtraction. In such situations, the background correction will remove at least part of the

real stratospheric SO₂ signal leading to an underestimation of the total SO₂ burden. This is an important limitation when trying to estimate SO₂ lifetime from the measurements but should not be critical for volcanic alert services.

3.5 Error Discussion and Validation

TBD

4 Retrieval Example: Kasatochi eruption August 2008

The Kasatochi Volcano (52.17°N, 175.51°W) is a small (2.7×3.3 km) unpopulated island volcano, situated on the Aleutian arc. The active stratovolcano reaches only 314 m above sea level, and the 750-m-wide crater contained a saltwater lake. On 7-8 August 2008, the Kasatochi volcano erupted with little warning. The eruption injected large amounts of SO₂ and ash into the atmosphere, a significant part of it reaching the stratosphere. While the ash particles were deposited after a few days, the SO₂ dispersed throughout the whole Northern Hemisphere and could be detected in satellite data for several weeks. In Fig. 13, GOME-2 measurements are shown for the first 6 days of the Kasatochi eruption. The volcanic debris was injected into a low pressure system resulting in a rotating movement of the plume which subsequently separated into different parts which rapidly moved over the North American continent. In the following days, more and more filaments formed eventually leading to enhanced SO₂ over most of the Northern Hemisphere.

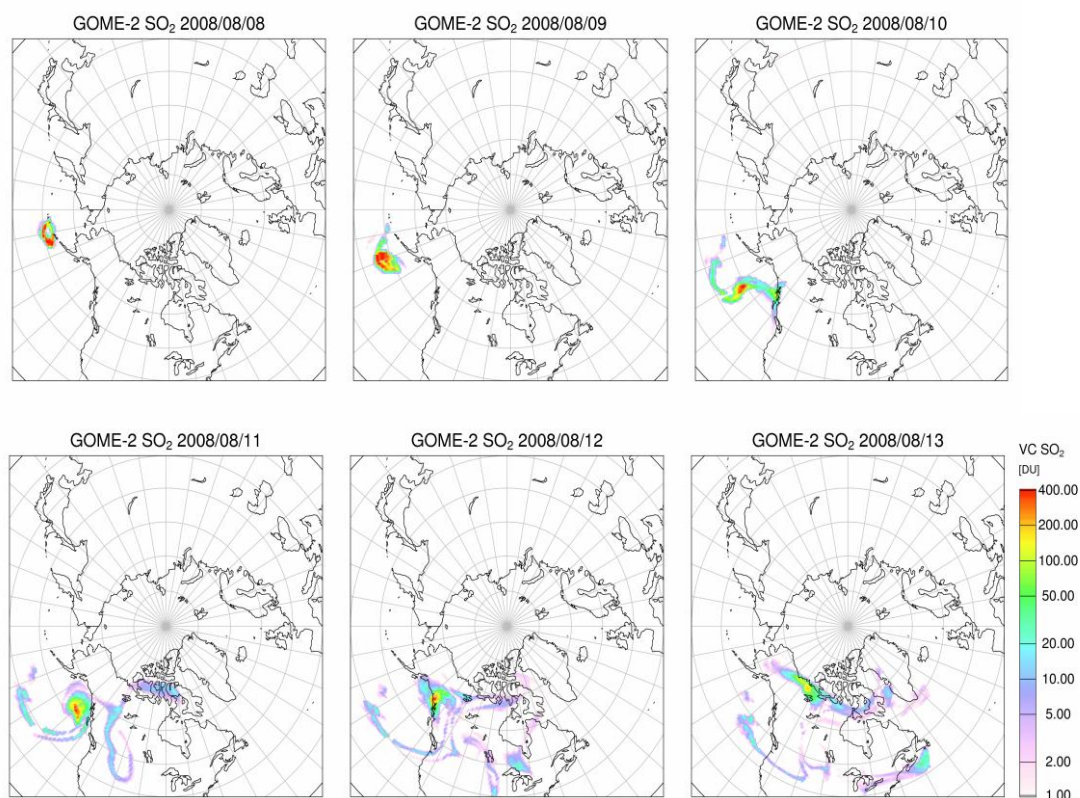


Fig. 13: Evolution of the Kasatochi SO₂ plume over the first 6 days as seen by GOME-2

5 Planned Improvements

A number of improvements are foreseen for the volcanic SO₂ product. In the short run, several relatively straight forward algorithm updates will be implemented, including

- Correction of line of sight effects
- Use of retrieved reflectance for the SOD lookup tables which will also provide a first order correction for the influence of clouds below the SO₂ plume

In the long run, options for retrieval of SO₂ layer height as suggested by Yang et al., 2009b will be evaluated. However, constraints on retrieval speed will probably exclude a full inversion in the NRT product.

Further improvements might become necessary depending on the results of validation activities foreseen in the SAVAA project and other studies.

6 Volcanic Alert System

The volcanic alert system is a demonstration system based on GOME-2 data and a very simple web interface. It is intended to demonstrate the GOME-2 capabilities for volcanic SO₂ detection and does not claim to be a real NRT application for use by aviation centres. It is currently operated on the IUP Bremen web page at http://www.doas-bremen.de/gome2_so2_alert.htm.

6.1 Identification of volcanic plumes

The main aim of the volcanic alert system is to reliably identify SO₂ from volcanic plumes with as high sensitivity as possible and as few false alerts as possible. An indication is also given for the estimated total SO₂ mass in the plume although that has a low accuracy as the height of the plume is not yet taken into account.

Alerts are raised on a fixed grid of 5° x 5°. For larger plumes, several alerts are raised on the same day. On the web interface, a global overview showing only the alerts is given and for each alert, a zoomed map showing the retrieved SO₂ field.

In order to separate between noise and real volcanic SO₂, the following criteria are applied to the measurements when selecting the values:

- SZA < 80
- Chisquare of the retrieval below threshold
- Only values which are larger than 5 times the RMS taken over the surrounding 51 values are considered as real. To estimate the RMS, only the negative values are used assuming that they represent the noise level and are not affected by real volcanic SO₂ measurements

An alert is raised if more than 4 pixels in one 5° x 5° box fulfil all the above conditions. This threshold will exclude small plumes but reduces the number of false alerts. A more stringent criterion will further reduce the number of false alerts, similarly as increasing the minimum threshold for peak identification.

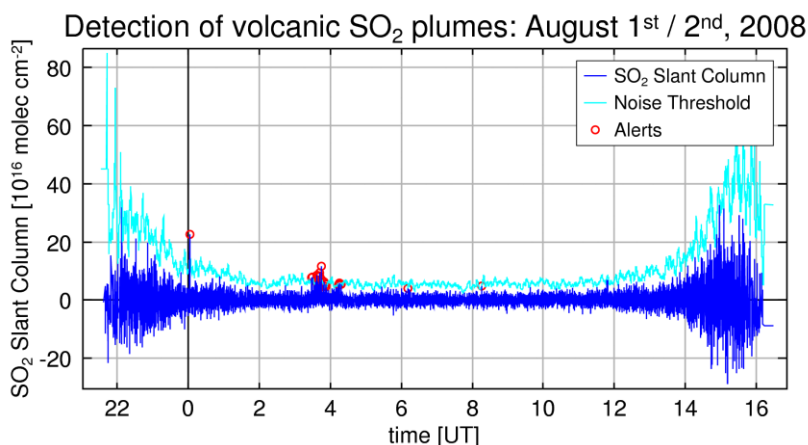


Fig. 14: Example of the volcanic alert identification on a single orbit of GOME-2 data. Shown are the SO₂ columns (dark blue), the noise threshold (cyan) and the alerts (red circles).

The complete GOME-2 data set was processed with the alert system. An overview on the number of alerts raised is given in Fig. 15. Please note that this is the number of 5° x 5° boxes for which an alert was raised and is not proportional to the number of satellite pixels for which the SO₂ column was flagged as being volcanic. Also, the number of alerts is not proportional to the total SO₂ mass emitted. As some of the SO₂ from the large eruptions was emitted into the stratosphere where it has a longer lifetime, one single eruption can lead to many alerts over the course of weeks.

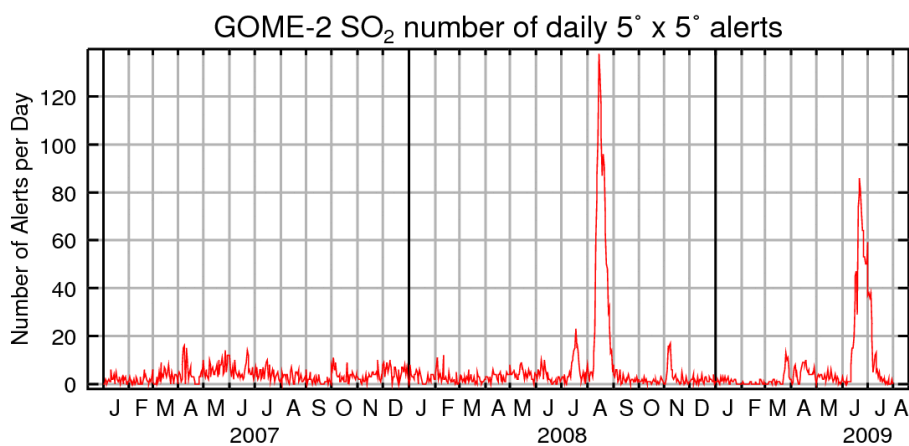


Fig. 15: Number of 5°x5° grid boxes for which an alert was raised for each day. The largest peaks can be linked to Okok, Aleuten Islands (July 2008), Kasatochi (August 2008), Dalaffilla (November 2008), Redoubt (March and April 2009), and Sarychev Peak (June and July 2009)

6.2 Web interface

The web interface is very basic and fully integrated into the web page of the DOAS group at the IUP Bremen. An example of the interface is shown in Fig. 16. Basically, the user can change the date either by stepping backwards or forwards by clicking on the arrows above the graphical display or by using the calendar to the right. The zoomed image below the main display can be selected interactively by clicking on the alerts highlighted in the global map.

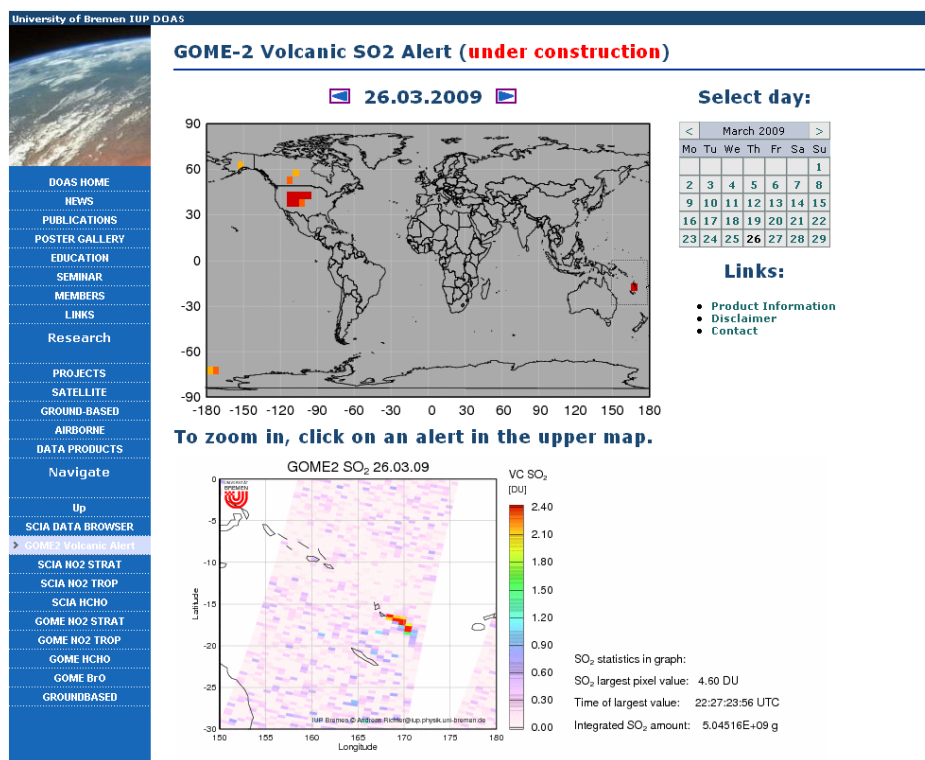


Fig. 16: Example of the GOME-2 alert page on the IUP Bremen web site
http://www.doas-bremen.de/gome2_so2_alert.htm.

The current implementation does not use any scripts and cookies. It therefore will not remember the last user settings even from day to day (it will e.g. not zoom automatically on the same region when changing date even if this has an alert as well). Also, it does not automatically open on the most recent day.

6.3 Open issues / plans for improvements

- False alerts are often raised at large SZA where the noise in the SO₂ data increases. This can be reduced by applying more strict thresholds albeit at the expense of reduced sensitivity
- Sometimes, tropospheric pollution is also picked up and detected as volcanic plume, in particular over China or the South African Power Plants. These vents are rare and can be identified based on their location
- The web interface will be complemented by a script based version providing a more user friendly interface and additional options.

7 Data Formats

The volcanic SO₂ processor currently produces three types of files:

1. The orbital swath files containing all the information on the individual GOME-2 pixels and the retrieved SO₂ column. There are about 14 such files per day, the average size being 2.5 Mbytes in binary format.
2. The daily alert files containing the number of alerts per 5° x 5° grid box. These files are in ASCII format and are about 15 Kbytes large.

- The daily images for the regions with alerts. These files are in GIF format and typically 40 KBytes large.

7.1 Format of swath files

Swath files are simple binary files consisting of a file header in ASCII format followed by the data given as single precision floating point numbers in little-endian format.

The first line of the header contains the file format identifier, the length of the header in bytes and the number of columns in the file, for example

```
*<Binary PC Slant File V1.00> 2932 40
```

In this file, the header is 2932 bytes long and the file contains 40 columns. The next lines (40 in the example file) contain the descriptions of the individual columns in the file, separated by CR and LF in DOS / WINDOWS style. The rest of the header contains additional information on the retrieval. The number of values in the file can be computed by

$$N_values = (FileSize - HeaderSize) / 4$$

Please note that the file format is dynamic in that both the number of columns and their order is not fixed but may change from one data version to the next. Therefore, it is recommended to parse the header to identify the columns of those data the user wishes to read. For historical reasons, the column description is partly in German. The most interesting columns are listed and translated in Tab. 3.

Label in file	Meaning	Column in file (might vary!)
* Uhrzeit [h]	Time UT in hours [0..24]	1
* Sonnen-Zenitwinkel [°]	Solar Zenith Angle in degrees	2
* Latitude [°]	Latitude of pixel centre in degrees	4
* Longitude [°]	Longitude of pixel centre in degrees	5
* SubSet [-64..64], < 0 = Back]	Subset position in scan, negative values denote back-scan	6
* LineOfSight [°]	Line of sight angle in degrees	7
* RelAzimuth [°]	Solar Azimuth in degrees	8
* Vertikale Spalte SO ₂ [DU]	Vertical Column SO ₂ in DU	11
* Fit-Fehler SO ₂ [%]	Fitting uncertainty of SO ₂ in %	1 ₂
* Lat1 [°]	Corner coordinates of satellite pixel	31
* Long1 [°]		3 ₂
* Lat ₂ [°]		33
* Long ₂ [°]		34
* Lat3 [°]		35
* Long3 [°]		36
* Lat4 [°]		37
* Long4 [°]		38
* FRESCO cloud cover [0..1]	FRESCO cloud cover [0..1]	39
* FRESCO cloud top pressure [mbar]	FRESCO cloud top pressure [mbar]	40

Tab. 3: Overview on most important columns in binary swath files

7.2 Format of alert files

The alert files are simple ASCII files having the extension '.ASP' which consists of a header of variable length followed by the data. This format is used for all gridded satellite products produced by the IUP Bremen DOAS group. The file contents are

- first a header of varying length with a * as first character in each line
- followed by blocks of data for the individual latitude bands from south to north. Each block starts with a line giving the centre latitude (this line again starts with a *) followed by a number of lines with the values for the individual longitudes from west to east.
- the latitude and longitude steps as well as the starting and ending values are given in the header
- all the values have to be multiplied by a factor also given in the header
- missing values are flagged with a value given in the header
- the files are in DOS / WINDOWS style using CR LF as end of line markers

8 Acronyms

AMF	Airmass Factor
CR	Carriage Return (13)
DOAS	Differential Optical Absorption Spectroscopy
GOME	Global Ozone Monitoring Experiment
GOME-2	Global Ozone Monitoring Experiment 2
LF	Line Feed (10)
NRT	Near Real Time
OMI	Ozone Monitoring Instrument
SAA	Southern Atlantic Anomaly
SCD	Slant Column Density
SCIAMACHY	Scanning Imaging Spectrometer for Atmospheric Chartography
SOD	Slant Optical Depth
SZA	Solar Zenith Angle
UV	Ultraviolet
VCD	Vertical Column Density

9 References

Afe, O. T., A. Richter, B. Sierk, F. Wittrock and J. P. Burrows, BrO Emission from Volcanoes - a Survey using GOME and SCIAMACHY Measurements, *Geophys. Res.Lett.*, **31**, L24113, doi:10.1029/2004GL020994, 2004

Carn S. A. , Krueger A. J. , Bluth G. J. S. , Schaefer S. J. , Krotkov N. A. , Watson I. M. , Datta S., Volcanic eruption detection by the Total Ozone Mapping Spectrometer (TOMS) instruments: a 22-year record of sulfur dioxide and ash emissions, In: Oppenheimer C, Pyle DM, Barclay J (eds) Volcanic degassing. *Geological Society, London, Special Publications*, **213**,177–202, 2003.

Carn, S. A., A. J. Krueger, N. A. Krotkov, K. Yang, and P. F. Levelt, Sulfur dioxide emissions from Peruvian copper smelters detected by the Ozone Monitoring Instrument, *Geophys. Res. Lett.*, **34**, L09801, doi:10.1029/2006GL029020, 2007.

Carn, S. A., N. A. Krotkov, K. Yang, R. M. Hoff, A. J. Prata, A. J. Krueger, S. C. Loughlin, and P. F. Levelt, Extended observations of volcanic SO₂ and sulfate aerosol in the stratosphere, *Atmos. Chem. Phys. Disc.*, **7**, 2857–2871, 2007.

DLR, Algorithm Theoretical Basis Document for GOME-2 Total Column Products of Ozone, Minor Trace Gases, and Cloud Properties (GDP 4.2 for O3M-SAF OTO and NTO)(http://wdc.dlr.de/sensors/gome2/DLR_GOME-2_ATBD_2A.pdf), 2009.

Eisinger, M., and J. P. Burrows, Tropospheric sulfur dioxide observed by the ERS-2 GOME instrument, *Geophys. Res. Lett.*, **25**, 4177–4180, 1998.

Eskes, H. J., and K. F. Boersma, Averaging kernels for DOAS total column satellite retrievals, *Atmos. Chem. Phys.*, **3**, 1285–1291, 2003.

Khokhar, M. F., C. Frankenberg, S. Beirle, S. Köhl, M. Van Roozendaal, A. Richter, U. Platt and T. Wagner, Satellite Observations of Atmospheric SO₂ from Volcanic Eruptions during the Time Period of 1996 to 2002, *Journal of Advances in Space Research*, **36**(5), 879–887, 10.1016/j.asr.2005.04.114, 2005

Krotkov, N. A., S. A. Carn, A. J. Krueger, P. K. Bhartia, and K. Yang, Band residual difference algorithm for retrieval of SO₂ from the Aura Ozone Monitoring Instrument (OMI), *IEEE Trans. Geosci. Remote Sens.*, **44**(5), 1259–1266, doi:10.1109/TGRS.2005.861932, 2006

Krotkov, M. A., B. McClure, R. R. Dickerson, S. A. Carn, C. Li, P. K. Bhartia, K. Yang, A. J. Krueger, Z. Li, P. Levelt, H. Chen, P. Wang, and D. R. Lu, Validation of SO₂ retrievals from the Ozone Monitoring Instrument (OMI) over NE China, *J. Geophys. Res.*, **113**, D16S40, doi:10.1029/2007JD008818, 2008.

Krueger, A., Sighting of El Chichon sulfur dioxide clouds with the Nimbus 7 total ozone mapping spectrometer, *Science*, **220**, 1377–1379, 1983.

Krueger, A., Walter, L., Bhartia, P., Schnetzler, C., Krotkov, N., Sprod, I., and Bluth, G., 1995: Volcanic sulfur dioxide measurements from the total ozone mapping spectrometer instruments, *J. Geophys. Res.* **100**, 14057–14076.

Lee, C., Richter, A., Weber, M., Burrows, J. P., SO₂ retrieval from SCIAMACHY using the weighting function DOAS (WFDOAS) technique: comparison with standard DOAS retrieval, *Atmos. Chem. Phys.*, **8**, 6137–6145, 2008

Lee, C., Martin, R. V., van Donkelaar, A., O’Byrne, G., Krotkov, N., Richter, A., Huey, G., Holloways, J. S., Retrieval of vertical columns of sulfur dioxide from SCIAMACHY and OMI: Air mass factor algorithm development and validation, *J. Geophys. Res.*, in press, 2009

McPeters, R., The atmospheric SO₂ budget for Pinatubo derived from NOAA-11 SBUV/2 spectral data, *Geophys. Res. Lett.* **18**, 1971–1974, 1993

Munro, R., Eisinger, M., Anderson, C., Callies, J., Corpaccioli, E., Lang, R., Lefebvre, A., Livschitz, Y., and Albinana, A. P.: GOME-2 on MetOp, *Proc. of The 2006 EUMETSAT Meteorological Satellite Conference*, Helsinki, Finland, 12–16 June 2006, EUMETSAT P.48, 2006.

Richter, A., F. Wittrock, and J. P. Burrows, SO₂ measurements with SCIAMACHY, paper presented at Atmospheric Science Conference, Eur. Space Agency Cent. for Earth Obs., Frascati, Italy, 8–12 May, 2006.

Thomas, W., T. Erbertseder, T. Ruppert, M. van Roozendaal, J. Verdebout, D. Balis, C. Meleti, and C. Zerefos, On the retrieval of volcanic sulfur dioxide emissions from GOME backscatter measurements, *J. Atmos. Chem.*, **50**, 295–320, doi:10.1007/s10874-005-5544-1, 2005.

Vandaele, A. C., Simon, P. C., Guilmot, J. M., Carleer, M., and Colin, R.: SO₂ absorption cross section measurement in the UV using a Fourier transform spectrometer, *J. Geophys. Res.*, **99**, 25 599–25 605, 1994.

Vountas, M., Rozanov, V. V., and Burrows, J. P.: Ring effect: Impact of rotational Raman scattering on radiative transfer in earth's atmosphere, *J. Quant. Spectrosc. Ra.*, **60**, 943–961, 1998.

Yang, K., N. A. Krotkov, A. J. Krueger, S. A. Carn, P. K. Bhartia, and P. F. Levelt, Retrieval of large volcanic SO₂ columns from the Aura Ozone Monitoring Instrument: Comparison and limitations, *J. Geophys. Res.*, **112**, D24S43, doi:10.1029/2007JD008825, 2007.

Yang, K., N. A. Krotkov, A. J. Krueger, S. A. Carn, P. K. Bhartia, and P. F. Levelt, Improving retrieval of volcanic sulfur dioxide from backscattered UV satellite observations, *Geophys. Res. Lett.*, **36**, L03102, doi:10.1029/2008GL036036, 2009a.

Yang, K., X. Liu, N. A. Krotkov, A. J. Krueger, and S. A. Carn, Estimating the altitude of volcanic sulfur dioxide plumes from space borne hyper-spectral UV measurements, *Geophys. Res. Lett.*, **36**, L10803, doi:10.1029/2009GL038025, 2009b.